

Numerical simulation of rarefied gas flow through a thin orifice

By FELIX SHARIPOV

Departamento de Física, Universidade Federal do Paraná, Caixa Postal 19044, 81531-990 Curitiba, Brazil
sharipov@fisica.ufpr.br

(Received 12 December 2003 and in revised form 1 June 2004)

Rarefied gas flow through a thin orifice is studied on the basis of the direct simulation Monte Carlo method. The mass flow rate and the flow field are calculated over the whole range of the Knudsen number for various values of the pressure ratio. It is found that at all values of the pressure ratio a significant variation of the flow rate occurs in the transition regime between the free-molecular and hydrodynamic regimes. In the hydrodynamic regime the flow rate tends to a constant value. In the case of finite pressure ratio the flow field qualitatively differs from that for outflow into vacuum, namely vortices appear in the downflow container on approaching the hydrodynamic regime. Then, in the hydrodynamic regime the gas flow forms a strong jet. A comparison of the numerical results with experimental data available in the open literature has been performed.

1. Introduction

Rarefied gas flow through a thin orifice is of great practical interest. This kind of flow is realized in vacuum equipment, see e.g. Dushman (1962); Roth (1976), microfluidics, see e.g. Aktas, Aluru & Ravaioli (2001), electronic microscopy, see e.g. Danilatos (2001), Danilatos, Phillips & Nailon (2001), spacecraft design, see e.g. Jamison, Ketsdever & Muntz (2002), metrology of gas flow, see e.g. Szwemin, Szymański & Jousten (1999), Jitschin, Weber & Hartmann (1995), Jitschin, Ronzheimer & Khodabakhshi (1999), and in many other applications. As was noted in the previous papers Sharipov & Seleznev (1998) and Sharipov (2002*b*), in spite of the great practical importance, till now no reliable results on orifice flow have been available in the open literature for wide ranges of the parameters determining the gas flow, namely gas rarefaction and the pressure drop through the orifice.

Below, we will distinguish the three regimes with respect to gas rarefaction. If the gas rarefaction is high and the molecular mean free path in the upflow container is significantly larger than the orifice radius, then the regime is called free molecular or collisionless. If the rarefaction is low, i.e. the mean free path is significantly smaller than the orifice radius, then the regime is called hydrodynamic. If the rarefaction is intermediate between the free-molecular and hydrodynamic regimes, then the flow is called transitional. Two limits can be considered with respect to the pressure drop. If the pressure in the downflow container is negligible compared with that in the upflow one it can be said that the gas outflows into vacuum. The opposite limit corresponds to the case when the pressure drop is significantly smaller than the average pressure.

A number of works, see e.g. Liepmann (1961), Narasimha (1961), Willis (1965), Rotenberg & Weitzner (1969), have proposed analytical expressions for the mass flow

rate near the free-molecular regime in the case of outflow into vacuum, which are valid in a very small range of gas rarefaction. Some numerical data for the outflow into vacuum in the transition regime are reported by Shakhov (1974) and Sharipov (2002*b*). In the hydrodynamic regime the problem was solved by Alder (1979) on the basis of the Euler equation, which is valid for high values of the Reynolds number. In the case of low Reynolds number Roscoe (1949) and Hasimoto (1958) solved the Stokes equation analytically. Thus, the theoretical results on orifice flow are restricted to small ranges of gas rarefaction and pressure drop.

Systematical experimental results on orifice flow in the hydrodynamic regime were reported by Perry (1949) for a large pressure drop and by Linden & Othmer (1949) for a small pressure drop. Some experimental results in the case of outflow into vacuum are presented by Liepmann (1961). However, in the transition regime the scatter of his experimental points is rather large which makes the data non-reliable. Sreerkanth (1965) presented experimental data for the transition regime at various values of the pressure drop. Borisov *et al.* (1973) and Porodnov *et al.* (1974) provide experimental results for a small pressure drop for a wide range of gas rarefaction. Barashkin, Porodnov & Chemagin (1977*a*), Barashkin, Porodnov & Suetin (1977*b*) and Jitschin *et al.* (1999) present experimental data on the outflow into vacuum through an orifice covering practically the whole range of gas rarefaction. Fujimoto & Usami (1984) reported experimental results on the mass flow rate through short tubes. The length-to-radius ratio of the shortest tube was $L/a = 0.05$, which can be considered an orifice. They measured the flow rate for a wide range of rarefaction for several values of the pressure drop. Thus, the experimental material on orifice flow is not as rich as one expects for such a type of gas flow.

The aim of the present paper is to calculate the mass flow rate and the flow field for a wide range of gas rarefaction for various values of the pressure ratio.

2. Statement of the problem and definitions

Consider an orifice in an infinitesimally thin partition, which separates two semi-infinite containers. One of them contains a gas at a pressure P_0 , while the other is maintained at a smaller pressure P_1 , i.e. $P_1 < P_0$. The temperatures of the gas in both containers are equal to T_0 . The quantity of practical interest is the mass flow rate \dot{M} through the orifice and the flow field in both containers.

The solution of the problem is determined by two main parameters: the pressure ratio P_1/P_0 and the gas rarefaction δ defined as

$$\delta = \frac{aP_0}{\mu_0 v_0}, \quad v_0 = \left(\frac{2kT_0}{m} \right)^{1/2}, \quad (2.1)$$

where a is the orifice radius, μ_0 is the stress viscosity at temperature T_0 , v_0 is the most probable molecular velocity at the same temperature, m is the molecular mass of the gas, and k is the Boltzmann constant. Considering the viscosity μ_0 to be proportional to the molecular mean free path ℓ one can see that the rarefaction parameter δ is inversely proportional to the Knudsen number defined as $Kn = \ell/a$. So, the limit $\delta = 0$ corresponds to the free-molecular (or collisionless) regime of the flow, while the opposite limit ($\delta \rightarrow \infty$) describes the hydrodynamic regime.

The rarefaction parameter δ can be related to the main dimensionless parameters of the gas dynamics, namely the Reynolds (Re) and Mach (Ma) numbers as

$$\delta = \frac{1}{\sqrt{2\gamma}} \frac{Re}{Ma}, \quad (2.2)$$

$$Re = \frac{a u \rho_0}{\mu_0}, \quad Ma = \frac{u}{c_0}, \quad c_0 = \left(\gamma \frac{kT_0}{m} \right)^{1/2}, \quad (2.3)$$

where γ is the specific heat ratio, u is a characteristics velocity of the gas flow, $\rho_0 = mP_0/kT_0$ is the mass density of the gas, and c_0 is the adiabatic sound velocity at temperature T_0 .

In the free-molecular regime $\delta = 0$ and under the condition $P_1/P_0 = 0$ the mass flow rate can be calculated analytically, see e.g. Bird (1994),

$$\dot{M}_0 = \frac{\sqrt{\pi} a^2}{v_0} P_0. \quad (2.4)$$

This expression can be used to introduce the reduced mass flow rate as

$$W = \frac{\dot{M}}{\dot{M}_0}, \quad (2.5)$$

which will be used henceforth. Assuming that in the free-molecular regime the opposite flows through the orifice do not interact with each other the total flow rate is easily obtained for an arbitrary pressure ratio P_1/P_0 :

$$W = 1 - \frac{P_1}{P_0} \quad \text{at} \quad \delta = 0. \quad (2.6)$$

If the partition thickness L is not infinitesimal but it is much smaller than the orifice radius, i.e. $L \ll a$, then according to Berman (1965) the flow rate given by (2.6) must be corrected to

$$W = \left(1 - \frac{P_1}{P_0} \right) \left(1 - \frac{L}{2a} \right). \quad (2.7)$$

3. Hydrodynamic regime

In the hydrodynamic limit $\delta \gg 1$ the problem can be solved on the basis of the continuum mechanics equations. Under the condition $Re \gg 1$ the gas flow can be considered as isentropic so that the Euler equation can be applied. The isentropic flow through an orifice can be considered as a limit case of nozzle flow. The mass flow rate through a nozzle \dot{M}_n is easily obtained from the Euler equation and can be written as

$$\dot{M}_n = 2\dot{M}_0 \left(\frac{P_1}{P_0} \right)^{1/\gamma} \left[\frac{\pi\gamma}{\gamma-1} \left(1 - \left(\frac{P_1}{P_0} \right)^{(\gamma+1)/2} \right) \right]^{1/2} \quad \text{at} \quad \frac{P_1}{P_0} > \left(\frac{P_1}{P_0} \right)_*, \quad (3.1)$$

and

$$\dot{M}_n = \dot{M}_0 \sqrt{2\pi\gamma} \left(\frac{2}{\gamma+1} \right)^{\frac{\gamma+1}{2(\gamma-1)}} \quad \text{at} \quad \frac{P_1}{P_0} \leq \left(\frac{P_1}{P_0} \right)_*, \quad (3.2)$$

where $(P_1/P_0)_*$ is the so-called critical pressure ratio given as

$$\left(\frac{P_1}{P_0} \right)_* = \left(\frac{2}{\gamma+1} \right)^{\gamma/(\gamma-1)}. \quad (3.3)$$

It is known that under the condition $(P_1/P_0) > (P_1/P_0)_*$ a decrease of P_1 leads to an increase of the flow rate if P_0 is fixed. However, under the condition $(P_1/P_0) < (P_1/P_0)_*$

Source	L/a	Gas	γ	C	W
Liepmann (1961)	0.0507	Ar	5/3	0.812	1.48
Barashkin <i>et al.</i> (1977b)	0.0420	Ar	5/3	0.826	1.50
Jitschin <i>et al.</i> (1999)	0.0162	He, Ar, Kr	5/3	0.853	1.55
Perry (1949)	0.151	air	1.4	0.843	1.45
Fujimoto & Usami (1984)	0.050	air	1.4	0.844	1.45
Liepmann (1961)	0.0478	N ₂	1.4	0.824	1.41
Barashkin <i>et al.</i> (1977b)	0.0420	H ₂	1.4	0.853	1.46
Jitschin <i>et al.</i> (1999)	0.0162	H ₂ , N ₂ , air	1.4	0.869	1.49
Alder (1979)	0	diatomic	1.4	0.830	1.42
Liepmann (1961)	0.0478	CO ₂	1.3	0.830	1.39
Barashkin <i>et al.</i> (1977b)	0.0420	CO ₂	1.3	0.856	1.43
Jitschin <i>et al.</i> (1999)	0.0162	CO ₂	1.3	0.891	1.49
Jitschin <i>et al.</i> (1999)	0.0162	C ₃ H ₈	1.13	0.876	1.41

TABLE 1. Discharge coefficient C and flow rate W in the hydrodynamic regime ($\delta \rightarrow \infty$) for outflow into vacuum ($P_1/P_0 = 0$) for various specific heat ratios γ .

a further decrease of P_1 does not change the flow rate so that the flow rate M_n given by (3.2) does not depend on the pressure ratio. The last situation is called a choked flow.

The expressions (3.1) and (3.2) were obtained assuming a gradual decrease of the nozzle cross-section that is not valid for the orifice flow. As a result the experimental works by Perry (1949), Liepmann (1961), Barashkin *et al.* (1977a,b), and Jitschin *et al.* (1999) reported a lower value of the flow rate than that given by (3.2). To characterize this discrepancy a discharge coefficient C was introduced as

$$C = \frac{\dot{M}}{\dot{M}_n}, \quad (3.4)$$

which is used in many papers on orifice flow. Thus, in the hydrodynamic regime ($\delta \rightarrow \infty$) for high Reynolds numbers the flow rate W through an orifice can be related to the discharge coefficient C as

$$W = C \frac{\dot{M}_n}{\dot{M}_0}. \quad (3.5)$$

The experimental data by Perry (1949), Liepmann (1961), Barashkin *et al.* (1977a,b), and Jitschin *et al.* (1999) and the theoretical results by Alder (1979) in the case $P_1/P_0 = 0$ are summarized in table 1. In the second column the ratio of the partition thickness L to the orifice radius a used in the experiments is given. The experimental data by Perry (1949); Fujimoto & Usami (1984) and the theoretical results by Alder (1979) on the discharge coefficient C for different values of the pressure ratio are presented in table 2. From these data we conclude that the dependence of the discharge coefficient C on the specific heat ratio γ is weaker than that of the flow rate. At the same time, the coefficient C significantly depends on the pressure ratio. However, the experimental results of different authors are not in good agreement with each other even for the same species of gas. For monatomic and diatomic gases the disagreement reaches 5% and for CO₂ the disagreement is 7%. This disagreement can be explained by the influence of the partition thickness. In the free-molecular

Source	γ	C			
		$P_1/P_0 = 0$	0.1	0.5	0.9
Perry (1949)	1.4	0.843	0.840	0.756	0.617
Fujimoto & Usami (1984)	1.4	0.844	0.836	0.757	–
Alder (1979)	1.4	0.830	0.829	0.740	0.610
Present work	5/3	0.835	0.830	0.742	0.632

TABLE 2. Discharge coefficient C in the hydrodynamic regime ($\delta \rightarrow \infty$) for various pressure ratios P_1/P_0 .

regime this influence is estimated by (2.7), while in the hydrodynamic limit it can be evaluated by solving numerically the Euler equation.

In the limit of small pressure drop ($P_0 - P_1 \ll P_0$) Roscoe (1949) and Hasimoto (1958) solved analytically the two-dimensional Stokes equation and obtained the following solution:

$$W = \frac{2\delta}{3\sqrt{\pi}} \left(1 - \frac{P_1}{P_0}\right). \quad (3.6)$$

However, as was shown by Sharipov (1996) this solution is valid for low values of the Reynolds number and as a consequence the pressure drop must satisfy a very strong condition, namely

$$\frac{P_0 - P_1}{P_0} \ll \frac{1}{\delta^2}, \quad (3.7)$$

which not normally fulfilled in practice. So, the solution (3.6) is restricted to very small ranges of the pressure difference.

It should be noted that in many books, see e.g. Roth (1976), the solution (3.1) and (3.2) is called viscous flow in spite of the fact that it does not depend on the gas viscosity. It would be correct if the solution (3.6) were called viscous flow, because it is determined by the viscosity, while the solution (3.1) and (3.2) should be called an isentropic flow.

4. Method of solution

Like the previous paper Sharipov (2002*b*), the problem in question was solved by the direct simulation Monte Carlo (DSMC) method proposed and described by Bird (1994), which consists of the numerical simulation of the movements and collisions of a large number of model particles. The gas flow region is divided into a network of cells having dimension such that the change in flow properties across each cell is small. The time is advanced in discrete steps of magnitude Δt , such that Δt is small compared with the mean time t_m between two successive collisions given by

$$t_m = \mu_0/P_0. \quad (4.1)$$

Initially, the model particles are distributed uniformly in each container with Maxwellian distribution functions corresponding to the equilibrium states far from the orifice. The positions and velocities of the particles are saved in a computer memory. Then, the particle motion and their collisions are uncoupled over the small time interval Δt by repetition of the following two stages.

During the first stage the particles are moved through a distance determined by their velocity and by the time increment Δt . If the trajectory crosses a solid surface a simulation of the gas–surface interaction is performed according to a given law. The number of particles passing through the orifice from the upflow container to the downflow one N^+ and the number of particles passing through the orifice in the opposite direction N^- are counted. Then, the flow rate is calculated from the number of particles passing through the orifice in both directions, i.e. via the quantity $(N^+ - N^-)$. New particles are generated at boundaries of the computational region with the corresponding Maxwellian distribution function. The particles leaving the computational region are removed from the computer memory.

In the second stage the number of pairs to be selected for intermolecular collisions is calculated as

$$N_{coll} = \frac{N_p \bar{N}_p F_N (\sigma_T v_r)_{max} \Delta t}{2V_C}, \quad (4.2)$$

where N_p is the number molecules in a cell during the last time interval Δt , \bar{N}_p is the average value of N_p during all previous intervals Δt , F_N is the number of real gaseous particles represented by one model particle, v_r is the relative velocity of two particles, σ_T is the total collision cross-section of particles, and V_C is the cell volume. The parameter $(\sigma_T v_r)_{max}$ represents the maximum value of the product σ_T and v_r , which is stored for each cell. Every selected pair is accepted as a collision if $\sigma_T v_r / (\sigma_T v_r)_{max} > R$, where R is a random number varying from 0 to 1. This condition provides more frequent collisions between faster particles.

The constant cross-section σ_T corresponds to the hard-sphere (HS) model of molecules. In this case the exact expression for the viscosity obtained by Pekeris & Alterman (1957) is

$$\mu = 1.016034 \frac{5}{16} \frac{\sqrt{\pi m k T}}{\sigma_T}, \quad (4.3)$$

i.e. the viscosity is proportional to \sqrt{T} . Assuming the hard-sphere model it is not necessary to specify a gas, but it is possible to carry out the calculations in dimensionless quantities and to provide the reduced flow rate W as function of the rarefaction parameter δ .

However, in reality the dependence of the viscosity on the temperature is slightly different from (4.3). In general, we may write

$$\mu(T) \propto T^\omega, \quad (4.4)$$

where $\omega > 0.5$. To take into account dependence $\mu(T)$ the variable hard-sphere (VHS) model is used, see Bird (1994, §4.3). The idea is to introduce a variable cross-section as

$$\sigma_T(v_r) = \frac{\sigma_{0T}}{\Gamma(5/2 - \omega)} \left(\frac{4kT_0}{mv_r^2} \right)^{2\omega-1}, \quad (4.5)$$

where σ_{0T} is a reference cross-section related to a reference temperature T_0 via the viscosity by (4.3), and $\Gamma(x)$ is the gamma function. So, the cross-section σ_T depends on the relative velocity v_r of colliding particles that provides the correct dependence of the viscosity on the temperature, i.e. (4.4). The viscosity index ω depends on the species of gas and is given Bird (1994, table A 1). For instance, under the standard conditions (101 325 Pa and 0°C) $\omega = 0.66, 0.81$ and 0.85 for helium, argon and xenon, respectively. Thus, if one uses the VHS model one has to specify the gas to be considered. In this case the results lose a certain universality.

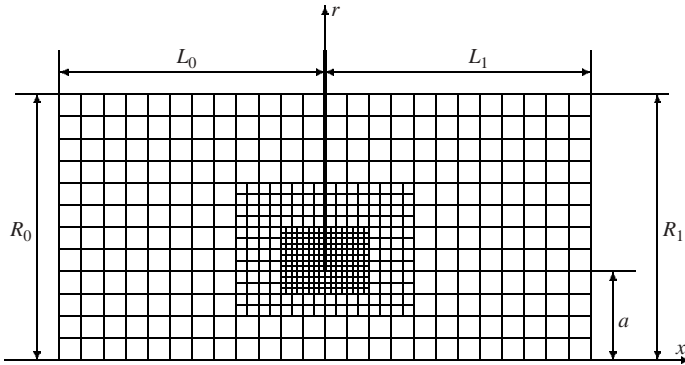


FIGURE 1. Coordinates and computational grid.

Some modifications were made to the program used in the previous papers Sharipov (2001), Sharipov (2002*b*) to improve the computational accuracy. First, a numerical grid of three levels with respect to the cell size was used in the present work as is shown in figure 1. Near the orifice edge where the variation of all quantities is sharp the cell size was smallest. The second improvement is related to the radial weighting factor. As Bird (1994) notes the most severe problem related to the DSMC method applied to axially symmetric flows is the small number of model particles in the cells located near the axis. In some situations an outermost cell has 100 times more particles than a central one. To reduce this difference the weighting factors were introduced. The computational region was divided in eight subregions having the form of coaxial cylinders. When particles pass from one subregion to another moving from the axis to the periphery, then half of the particles double their weight, while the other half is eliminated. When a particle moving from the periphery to the axis crosses the boundary between the subregions it is split into two particles each of half the weight. Such a procedure allows us to maintain a more uniform distribution of the model particles over the whole region of the gas flow. As a consequence, the statistical scattering of the flow rate is reduced significantly while maintaining the same number of model particles.

5. Gas–surface interaction

On the solid surface restricting the gas flow the distribution function satisfies a boundary condition, which in general form is expressed via a scattering kernel $R(\mathbf{v}' \rightarrow \mathbf{v})$, see Cercignani (1988),

$$|v_n| f(\mathbf{v}) = \int_{v'_n < 0} |v'_n| R(\mathbf{v}' \rightarrow \mathbf{v}) f(\mathbf{v}') d\mathbf{v}', \quad (5.1)$$

where \mathbf{v}' and \mathbf{v} are the molecular velocities of the incident and reflected particles, respectively, and v_n is the normal component of the velocity \mathbf{v} directed into the gas. As was shown in Sharipov (2002*a*, 2003*a,b*) the widely used diffuse–specular model of the gas–surface interaction contradicts some experimental data, while the model proposed by Cercignani & Lampis (1971) provides a more physical description of the gas scattering on a solid surface. The scattering kernel of this

model is

$$R(\mathbf{v}' \rightarrow \mathbf{v}) = \frac{m^2 v_n}{2\pi\alpha_n \alpha_t (2 - \alpha_t) (kT_w)^2} \times \exp \left\{ -\frac{m[v_n^2 + (1 - \alpha_n)v_n'^2]}{2kT_w\alpha_n} - \frac{m[\mathbf{v}_t - (1 - \alpha_t)\mathbf{v}_t']^2}{2kT_w\alpha_t(2 - \alpha_t)} \right\} I_0 \left(\frac{\sqrt{1 - \alpha_n} m v_n v_n'}{\alpha_n k T_w} \right), \quad (5.2)$$

where

$$I_0(x) = \frac{1}{2\pi} \int_0^{2\pi} \exp(x \cos \phi) d\phi,$$

\mathbf{v}_t is the two-dimensional vector of the tangential velocity, and T_w is the wall temperature.

The kernel (5.2) contains the two parameters α_t and α_n . The first has the physical meaning of the accommodation coefficient of the tangential momentum and the second is the accommodation coefficient of the kinetic energy corresponding to the normal molecular velocity. One can verify that if both accommodation coefficients are equal to unity the kernel (5.2) corresponds to diffuse scattering. In the other limit $\alpha_t = 0$ and $\alpha_n = 0$ the kernel (5.2) becomes the specular one. Moreover, it allows backscattering at $\alpha_t = 2$ and $\alpha_n = 0$, i.e. a particle changes the sign of its velocity after a collision with the surface.

In the present work this model is used to investigate the dependence of the orifice flow on the the gas–surface interaction. Four situations are considered: (i) $\alpha_t = 0$ and $\alpha_n = 0$, i.e. totally specular reflection; (ii) $\alpha_t = 0.5$ and $\alpha_n = 1$, i.e. partially specular and partially diffuse reflection; (iii) $\alpha_t = 1$ and $\alpha_n = 1$, i.e. totally diffuse scattering, and (iv) $\alpha_t = 2$ and $\alpha_n = 0$, i.e. back reflection. Note, the second and fourth situations cannot be modelled using the diffuse–specular scattering model.

6. Numerical accuracy

The calculations were carried out for four values of the pressure ratio P_1/P_0 : 0, 0.1, 0.5, and 0.9. The first value corresponds to outflow into vacuum. Some results were presented in Sharipov (2001, 2002*b*). So, this case is characterized as a strong non-equilibrium flow. The second value of P_1/P_0 also corresponds to a strong non-equilibrium flow, but this case allows us to study the influence of the presence of small quantity of the gas in the downflow container. The first and second values of the pressure ratio correspond to choked flow in the hydrodynamic regime ($\delta \rightarrow \infty$), since they satisfy the condition $(P_1/P_0) < (P_1/P_0)_*$. The third value is very close to the critical pressure ratio, which is equal to 0.487 for a monatomic gas in accordance with (3.3). Thus, this case represents a transition between choked and non-choked flow. Finally, the gas flow at the fourth value of P_1/P_0 can be characterized as a weakly non-equilibrium one. In this case the relative pressure drop $(P_0 - P_1)/P_0$ is equal to 0.1, i.e. it is sufficiently small.

The computational accuracy is determined by the following factors: space discretization, i.e. the cell size; the time discretization, i.e. Δt ; the size of the computational region; the number of simulated particles; and the number of samples used to calculate the macroscopic quantities.

Our aim was to maintain the computational error of the mass flow rate W within 1%. From carrying out some test calculations the following optimum parameters were

found. The size of the largest cell was $\Delta x = \Delta r = a/12$. Note, near the orifice edge the cell size was four times smaller, see figure 1. The time increment was $\Delta t = 0.01t_m$, where t_m is given by (4.1). The size of computational region was $R_0 = L_0 = R_1 = L_1 = 8a$, see figure 1. The test calculations were carried out for the four values of the gas rarefaction $\delta = 0.1, 1, 10$, and 100 and for all values of the pressure ratio P_1/P_0 considered, using the following parameters: $\Delta x = \Delta r = a/16$, $\Delta t = 0.002t_m$, $R_0 = L_0 = R_1 = L_1 = 12a$. In all these cases the variation of the flow rate W due to the variations of the grid parameters was less than 1%, i.e. within the computational error.

The number of simulated particles fluctuates during the calculation. It was maintained in the interval from 5×10^6 to 15×10^6 depending on the available computer memory. A comparison of results obtained for 5×10^6 particles with those obtained for 15×10^6 showed that 5×10^6 provides the assumed numerical error of 1%.

Special attention should be paid to the number of samples needed to reduce the statistical scattering. The fluctuation of the number of particles crossing the orifice from the upflow container to the downflow is of order $\sqrt{N^+}$. For the particles crossing the orifice in the opposite direction the fluctuation is about $\sqrt{N^-}$. Since the flow rate is calculated via the difference $N^+ - N^-$ the relative scattering of the flow rate will have the order $(\sqrt{N^+} + \sqrt{N^-})/(N^+ - N^-)$. Taking into account that $N^+ > N^-$ the relative scattering can be estimated as $\sqrt{N^+}/(N^+ - N^-)$. Thus, to guarantee the statistical scattering of the flow rate to be less than 1% every calculation must be continued until the condition

$$\frac{\sqrt{N^+}}{N^+ - N^-} < 0.001 \quad (6.1)$$

is satisfied. Since N^- increases on increasing the pressure ratio from 0 to 1, then the number of samples needed to satisfy the condition (6.1) drastically increases. Since for the pressure ratios $P_1/P_0 = 0$ and 0.1 we have $N^+ \gg N^-$, of the order 10^4 samples was enough. For the intermediate pressure ratio $P_1/P_0 = 0.5$ the number of samples increased to 10^5 . Finally, for the small pressure drop, i.e. $P_1/P_0 = 0.9$, 10^6 samples were necessary to satisfy the condition (6.1), because in this case N^- is very close to N^+ . These numbers of samples were obtained for 10^7 model particles. If one tried to apply the DSMC method for a smaller pressure drop, i.e. the pressure ratio closer to unity, the number of samples needed to maintain a reasonable statistical scattering would be huge, i.e. unachievable in practice. So, the value $P_1/P_0 = 0.9$ is a limit for application of the DSMC method using modern computers. In the range $0.9 < P_1/P_0 < 1$, i.e. for a small pressure drop, the gas flow through an orifice must be calculated by applying the kinetic equation as in Cercignani & Sharipov (1992), Sharipov (1996, 1997) and Hasegawa & Sone (1991).

7. Results and discussions

7.1. Flow rate

The numerical results on the reduced flow rate W are represented in figure 2 by the open symbols, where the rarefaction parameter δ varies from 0.1 to 250. It was found that at the smallest value $\delta = 0.1$ the deviation of the flow rate from its free molecular value is less than 2%, i.e. it is very close to the numerical error. For $\delta > 100$ no variations of the flow rate within the numerical accuracy were observed for all pressure ratios considered here. Therefore the data presented here cover the whole range of gas rarefaction δ .

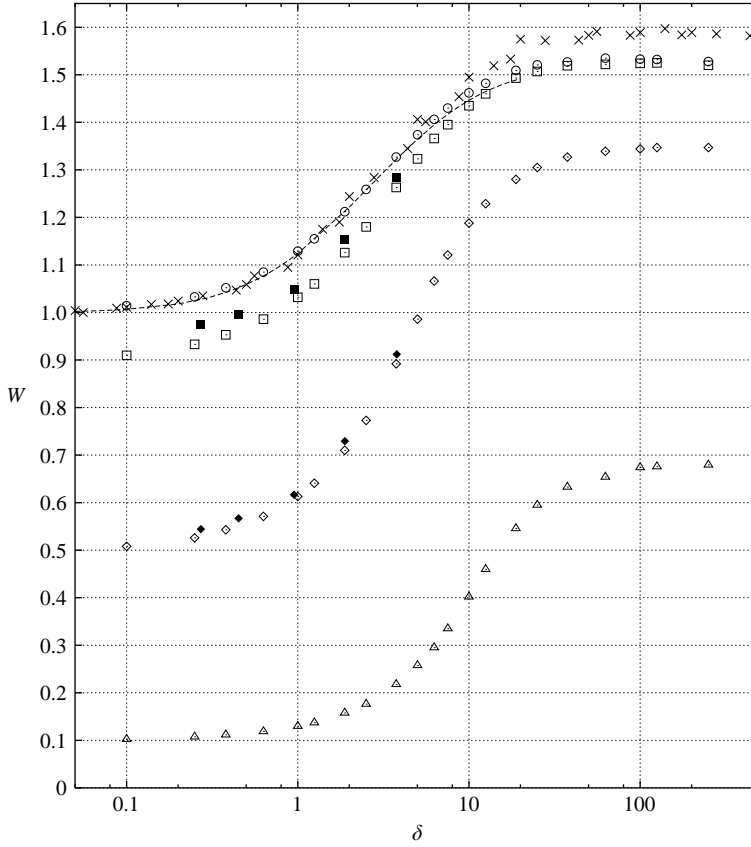


FIGURE 2. Reduced flow rate W vs. rarefaction parameter δ : \circ , $P_1/P_0=0$; \square , $P_1/P_0=0.1$; \diamond , $P_1/P_0=0.5$; \triangle , $P_1/P_0=0.9$ (open symbols, present work; filled symbols, experimental data by Sreekanth 1965); \times , experimental data by Jitschin *et al.* (1995); ----, empirical formulae by Fujimoto & Usami (1984) (equation (7.2)).

In the free-molecular regime ($\delta=0$), the numerical value of W tends to its theoretical value $W=(1-P_1/P_0)$. In many practical applications it is necessary to know the correction to this limit value related to the intermolecular collisions. Near the free-molecular regime the flow rate W can be written as

$$W = \left(1 - \frac{P_1}{P_0}\right) (1 + A\delta). \quad (7.1)$$

The constant A can be found from a comparison of the numerical results with (7.1) as presented in figure 3. One can see that the best-fit values of the constant A are 0.13, 0.15, 0.23 and 0.31 for the pressure ratio $P_1/P_0=0, 0.1, 0.5$ and 0.9 , respectively.

In the hydrodynamic regime ($\delta \rightarrow \infty$), the flow rate W also tends to a constant value, which depends on the pressure ratio P_1/P_0 . As has been mentioned above, in this limit the flow rate W can be related to the discharge coefficient C by (3.5). The numerical values of this coefficient are given in table 2 in §3 and compared with the experimental data by Perry (1949) and Fujimoto & Usami (1984) and with the theoretical results by Alder (1979). It can be seen that the values of C obtained in the present work are in a good agreement with those obtained by Alder (1979) in

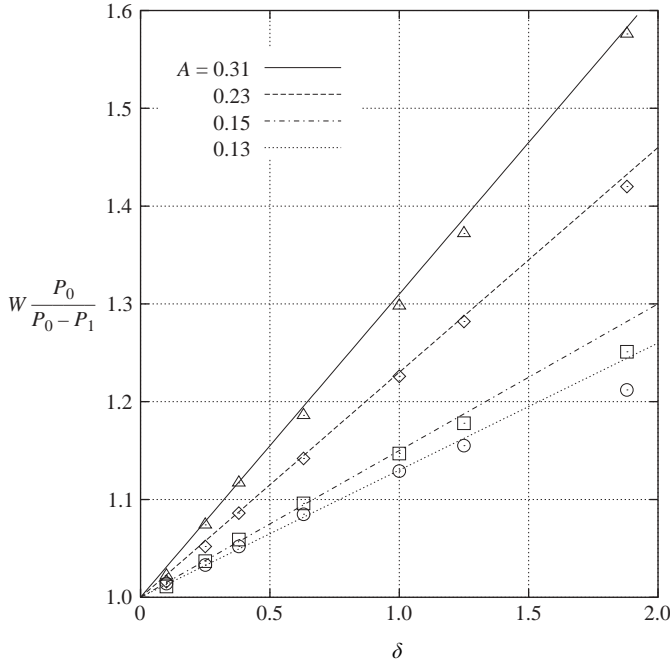


FIGURE 3. Comparison of the numerical results with (7.1) near the free-molecular regime:
 \circ , $P_1/P_0=0$; \square , $P_1/P_0=0.1$; \diamond , $P_1/P_0=0.5$; \triangle , $P_1/P_0=0.9$.

spite of the fact that he assumed a different value of the specific heat ratio γ . The experimental data by Perry (1949) and Fujimoto & Usami (1984) on the coefficient C slightly differ from the theoretical results, which can be explained by the finite thickness of partitions in the experiments.

A significant variation of the flow rate occurs for rarefaction parameter δ from 0.5 to 50 for any pressure ratio P_1/P_0 . The relative variation of the mass flow rate increases on increasing the pressure ratio. In the case of outflow into vacuum ($P_1/P_0=0$) the value of the flow rate W in the hydrodynamic regime ($\delta \rightarrow \infty$) is 1.5 times larger than its value in the free molecular regime ($\delta=0$), while for the pressure ratio $P_1/P_0=0.9$ the flow rates increases 6.6 times in the transition from $\delta=0$ to $\delta=100$.

Fujimoto & Usami (1984) proposed the following empirical formula based on their experimental data for outflow into vacuum:

$$W = 1 + \frac{0.4733 + 0.6005/\sqrt{\delta}}{1 + 4.559/\delta + 3.094/\delta^2}, \quad (7.2)$$

which is valid in the range $0 \leq \delta \leq 20$. This formula is presented in figure 2 by the dashed line. The experimental values for $P_1/P_0=0$ for the monatomic gases helium, argon and krypton measured by Jitschin *et al.* (1999) are shown in figure 2 by the crosses. One can see that in the range $0 \leq \delta \leq 10$ the empirical formula by Fujimoto & Usami (1984), the data by Jitschin *et al.* (1999) and the present theoretical results are in good agreement. In the range $10 \leq \delta \leq 250$ the experimental data by Jitschin *et al.* (1999) are systematically higher than the present theoretical results. The disagreement is about 5%, which exceeds the experimental uncertainty (2%) and the numerical error (1%). The experimental data on the outflow of argon into vacuum reported

		W				
		HS				VHS
P_1/P_0	δ	$\alpha_t = 0$ $\alpha_n = 0$	$\alpha_t = 0.5$ $\alpha_n = 1$	$\alpha_t = 1$ $\alpha_n = 1$	$\alpha_t = 2$ $\alpha_n = 0$	$\alpha_t = 1$ $\alpha_n = 1$
0	0.1	1.010	1.010	1.014	1.010	1.014
	1	1.122	1.129	1.129	1.119	1.115
	10	1.420	1.454	1.462	1.448	1.446
	100	1.488	1.523	1.534	1.540	1.531
0.1	0.1	0.911	0.910	0.910	0.913	0.910
	1	1.028	1.034	1.032	1.024	1.020
	10	1.391	1.426	1.435	1.454	1.415
	100	1.471	1.514	1.524	1.536	1.521
0.5	0.1	0.511	0.508	0.509	0.506	0.507
	1	0.609	0.613	0.613	0.604	0.603
	10	1.123	1.173	1.188	1.190	1.160
	100	1.251	1.326	1.344	1.369	1.344
0.9	0.1	0.1029	0.1029	0.1025	0.1026	0.1022
	1	0.1283	0.1289	0.1297	0.1275	0.1271
	10	0.3873	0.3997	0.4015	0.3978	0.3701
	100	0.5762	0.6578	0.6741	0.6861	0.6703

TABLE 3. Reduced flow rate W vs. rarefaction parameter δ , pressure ratio P_1/P_0 , accommodation coefficients α_t and α_n , and intermolecular potential: HS – hard spheres, VHS – variable hard spheres.

by Barashkin *et al.* (1977b) are slightly lower than the present theoretical results in the hydrodynamic regime, see table 1. However, this disagreement is within the experimental uncertainty, i.e. 2%.

The experimental data for the two values of the pressure ratio $P_1/P_0 = 0.1$ and 0.5 reported by Sreekanth (1965) are shown in figure 2 by the filled symbols. The present numerical results are in good agreement with the experimental data.

7.2. Influence of the gas–surface interaction

To study the dependence of the flow rate on the gas–surface interaction some calculations were carried out for non-diffuse scattering using the Cercignani–Lampis scattering kernel (5.2). A comparison of these results with those obtained for diffuse reflection is presented in table 3. The third column corresponds to completely specular reflection, the fourth column represents scattering intermediate between specular and diffuse, the fifth column shows the data for diffuse reflection and the results for back reflection are given in the sixth column. All these data were obtained for the hard-sphere model of intermolecular interaction. Naturally, the totally specular and back reflections are never realized in practice. However, considering these two limits it is possible to establish the variation of the flow rate due to the gas–surface interaction.

From table 3 it can be seen that near the free-molecular regime ($\delta = 0.1$) and in the transition ($\delta = 1$) regime the influence of the gas–surface interaction is of about the numerical accuracy. Near the hydrodynamic regime ($\delta = 10$) its influence reaches 6% and in the hydrodynamic regime ($\delta = 100$) its influence is about 16%. Thus, this is the maximum variation of the flow rate due to the gas–surface interaction that can

occur theoretically. However, in practice the variation range of the accommodation coefficients α_t and α_n is not as large as found here. As shown by Sharipov (2003a, b) the experimental value of the coefficient α_t varies for different gases in the range $0.85 \leq \alpha_t \leq 1$, while the coefficient α_n does not influence the mass flow rate. A more significant deviation from diffuse reflection takes place for atomically clean surfaces (Sazhin, Borisov & Sharipov 2001). Even in this case the reflection is far from specular. If one compares the data presented in the fourth and fifth columns of table 3, which embrace the real values of the accommodation coefficients, one can see that the strongest influence (about 2%) of the gas–surface interaction is observed for $\delta = 100$ and $P_1/P_0 = 0.9$. In all other situations the influence does not exceed the numerical accuracy.

Thus, in practice the influence of the gas–surface interaction on the flow rate through an orifice is very weak. This features of the orifice flow rate can be successfully used to test numerical methods in rarefied gas dynamics: practical numerical calculations can be carried out assuming diffuse scattering even if the real gas–surface interaction is not diffuse.

7.3. Influence of the intermolecular potential

To verify the sensitivity of the mass flow rate to the intermolecular potential some calculations were carried out for the VHS model using the molecular cross-section given by (4.5). The viscosity index ω was assumed to be 0.66, which corresponds to helium. The results of these calculations are presented in the seventh column of table 3, from which it can be seen that for $P_1/P_0 = 0$ and 0.1, the influence of the molecular model is about the numerical error, i.e. 1%. For the pressure ratio $P_1/P_0 = 0.5$ the influence slightly exceeds the numerical error at $\delta = 10$. However, for the small pressure drop, i.e. $P_1/P_0 = 0.9$ the flow rate becomes sensitive to the molecular model. Near the hydrodynamic regime $\delta = 10$ the variation of the flow rate W due to the molecular model reaches 8%.

At all the pressure ratios considered here the limit value of the flow rate W at $\delta \rightarrow \infty$ is not sensitive the molecular model.

7.4. Flow field

The streamlines for the four values of the rarefaction parameter δ are given in Figures 4, 5, 6, and 7 at $P_1/P_0 = 0, 0.1, 0.5,$ and 0.9 , respectively.

In the case of outflow into vacuum ($P_1/P_0 = 0$) the streamlines are as expected. Near the free-molecular regime ($\delta = 0.1$) they are symmetric. In the transition from the free-molecular regime to the hydrodynamic regime the symmetry is broken, but no qualitative change occurs.

For $P_1/P_0 = 0.1$ the behaviour of the streamlines is similar to that for $P_1/P_0 = 0$ near the free-molecular ($\delta = 0.1$) and in the transition ($\delta = 1$) regimes, while at $\delta = 10$ and 100 the behaviour is quite different. At $\delta = 10$ the gas begins to form vortices in the downflow container. In the hydrodynamic regime ($\delta = 100$) a jet of gas is observed in the downflow container. It can be seen that in the region $2 \leq x/a \leq 4$ and $0 \leq r/a \leq 0.5$ the streamlines are not straight but deviate from the x -axis.

For the pressure ratio $P_1/P_0 = 0.5$ the streamlines are not symmetric near the free-molecular regime $\delta = 0.1$, while they are symmetric in the transition regime ($\delta = 1$). Like the previous case, i.e. $P_1/P_0 = 0.1$, at $\delta = 10$ there are vortices at $\delta = 10$ and a jet is formed in the downflow container at $\delta = 100$. However, in this case the streamlines are straight.

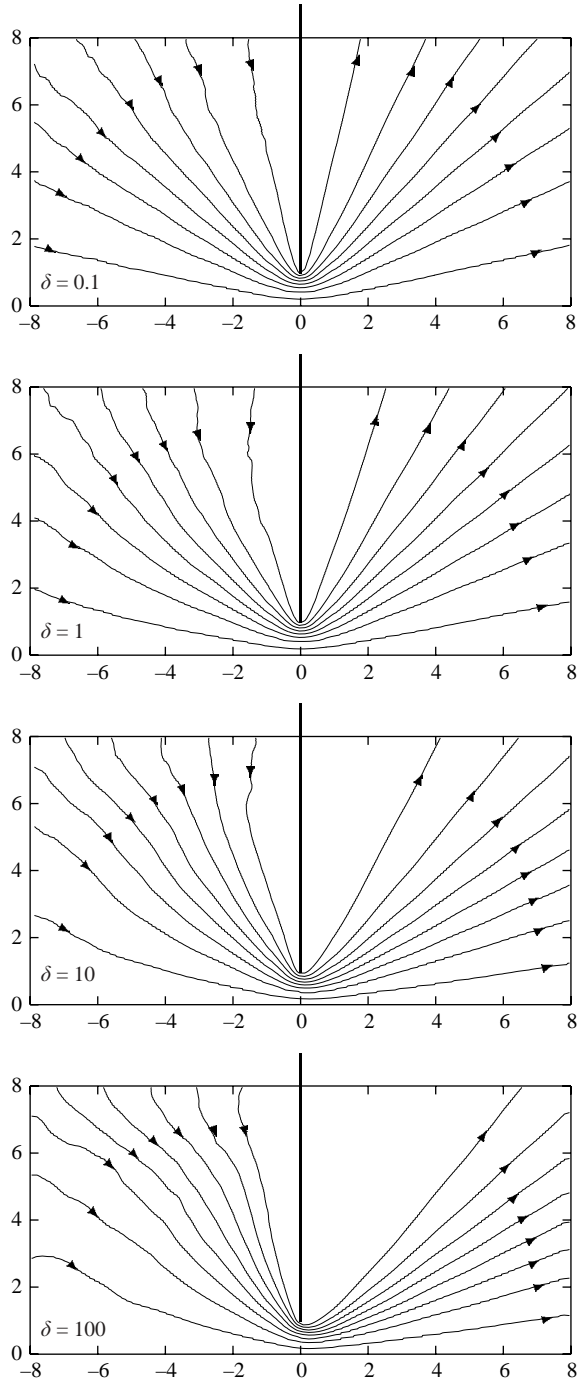


FIGURE 4. Streamlines at $P_1/P_0 = 0$.

For the small pressure drop, i.e. $P_1/P_0 = 0.9$, the behaviour of the streamlines is similar to that for $P_1/P_0 = 0.5$ at $\delta = 1, 10$ and 100 , while near the free-molecular regime ($\delta = 0.1$) the streamlines are quite different. This is an unexpected result. To eliminate doubt that this is a numerical phenomenon several calculations were

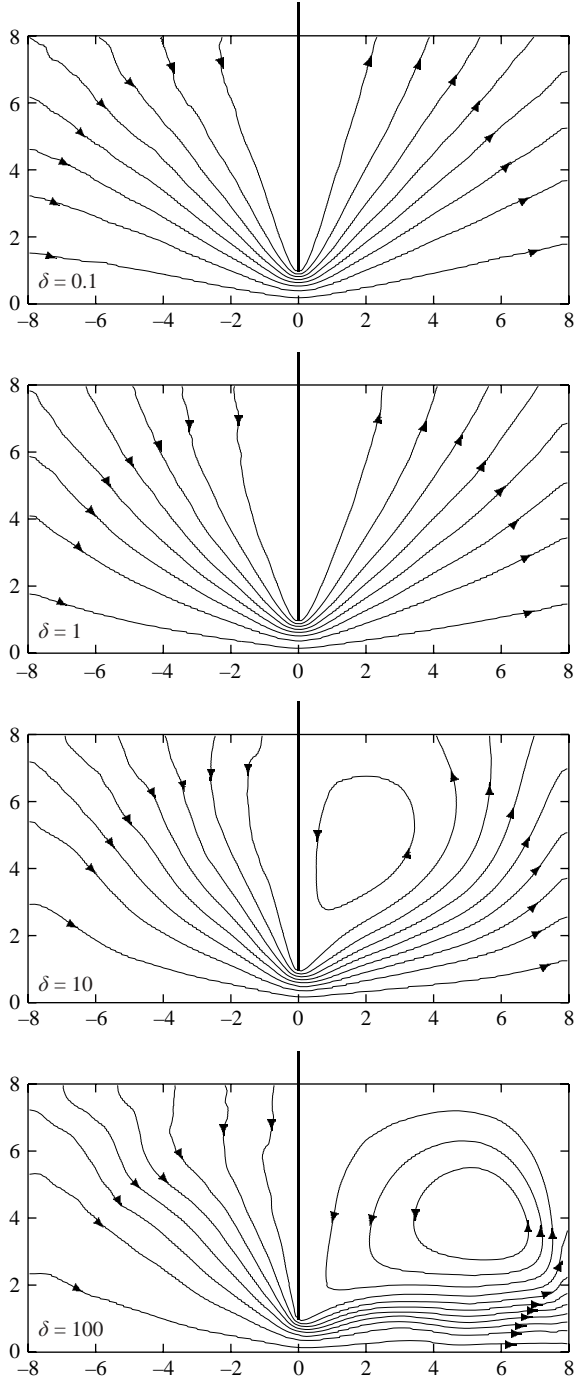


FIGURE 5. Streamlines at $P_1/P_0 = 0.1$.

carried out with different grid parameters, but the picture given in figure 7 for $\delta = 0.1$ is very stable. To confirm that this is really a physical phenomenon the corresponding calculations based on the kinetic equation should be carried out.

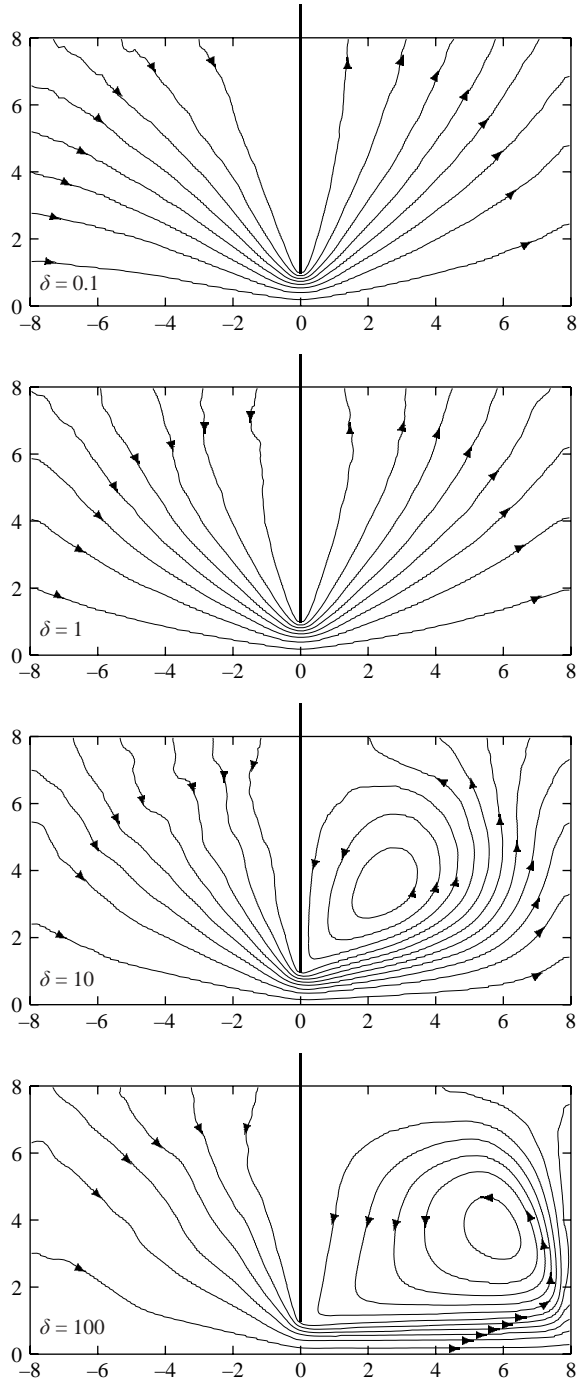


FIGURE 6. Streamlines at $P_1/P_0=0.5$.

The distributions of the density, temperature and longitudinal component of the bulk velocity along the symmetry axis are presented in figures 8, 9, 10, and 11 for the pressure ratios $P_1/P_0=0, 0.1, 0.5$, and 0.9 , respectively.

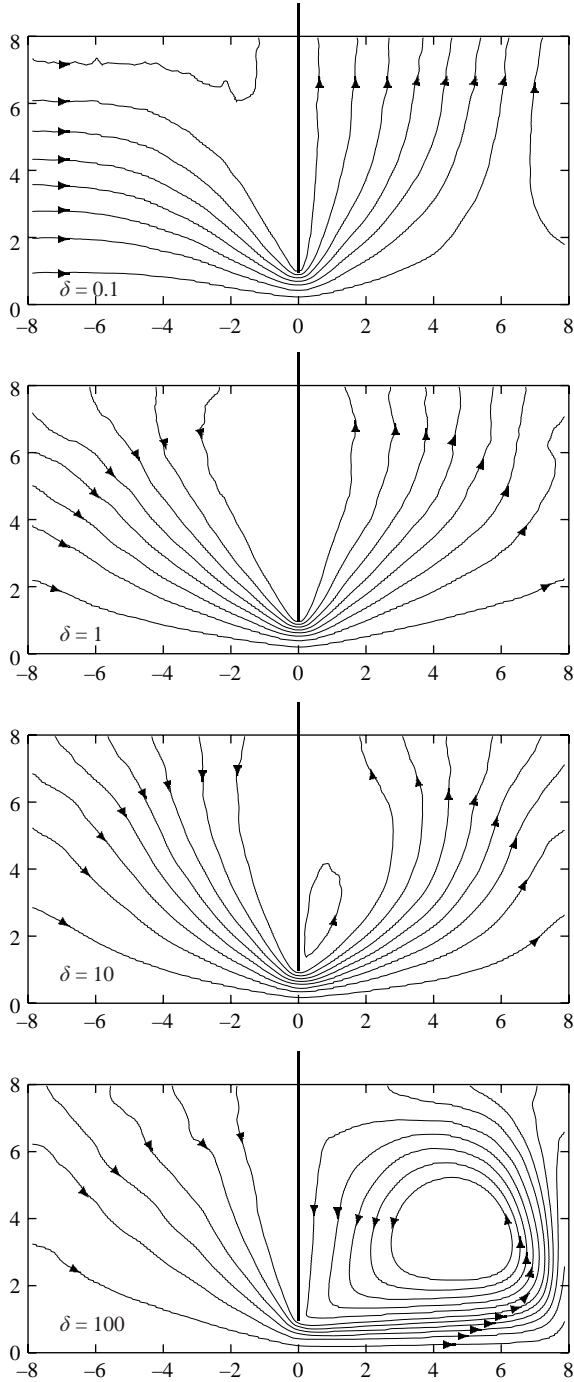


FIGURE 7. Streamlines at $P_1/P_0 = 0.9$.

In the case of outflow into vacuum ($P_1/P_0 = 0$) monotonic variations of the density and temperature from their equilibrium values n_0 and T_0 to zero are observed. The bulk velocity monotonically increases beginning from zero.

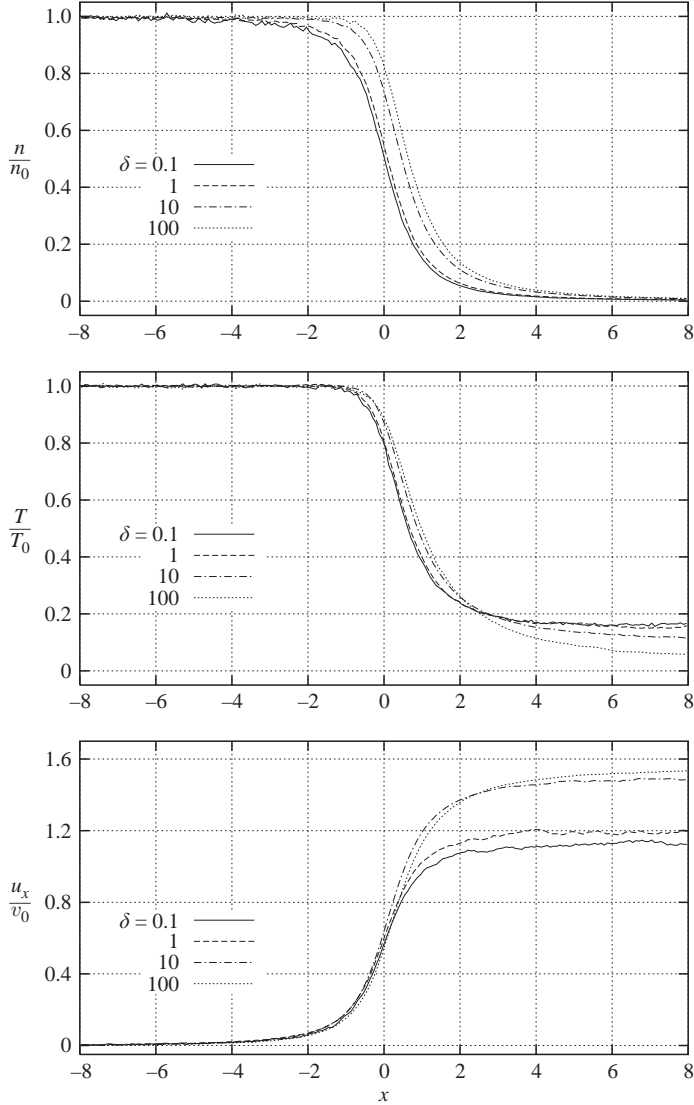


FIGURE 8. Distributions of density, temperature and bulk velocity along the orifice axis at $P_1/P_0 = 0$.

For the pressure ratio $P_1/P_0 = 0.1$ the density distribution monotonically decreases from n_0 to $0.1n_0$ for $\delta = 0.1, 1$ and 10 . The temperature of the gas has a minimum near the point $x/a = 1$ and then it tends to its equilibrium value T_0 at $\delta = 0.1, 1$, and 10 . In the hydrodynamic regime ($\delta = 100$) a non-monotonic behaviour of the density is observed. A similar behaviour of the density distribution along the orifice axis was noted in the experiments by Maté, Tejada & Montero (1998), Ramos *et al.* (2000) and Maté *et al.* (2001). The corresponding temperature has a very low value, i.e. $0.2T_0$ at the point $x/a = 3$ and then it non-monotonically increases up to the equilibrium value T_0 . It is curious that the bulk velocity distribution behaves oppositely to the temperature. It has a maximum at the point $x/a = 1$ at $\delta = 0.1, 1$ and 10 , then it

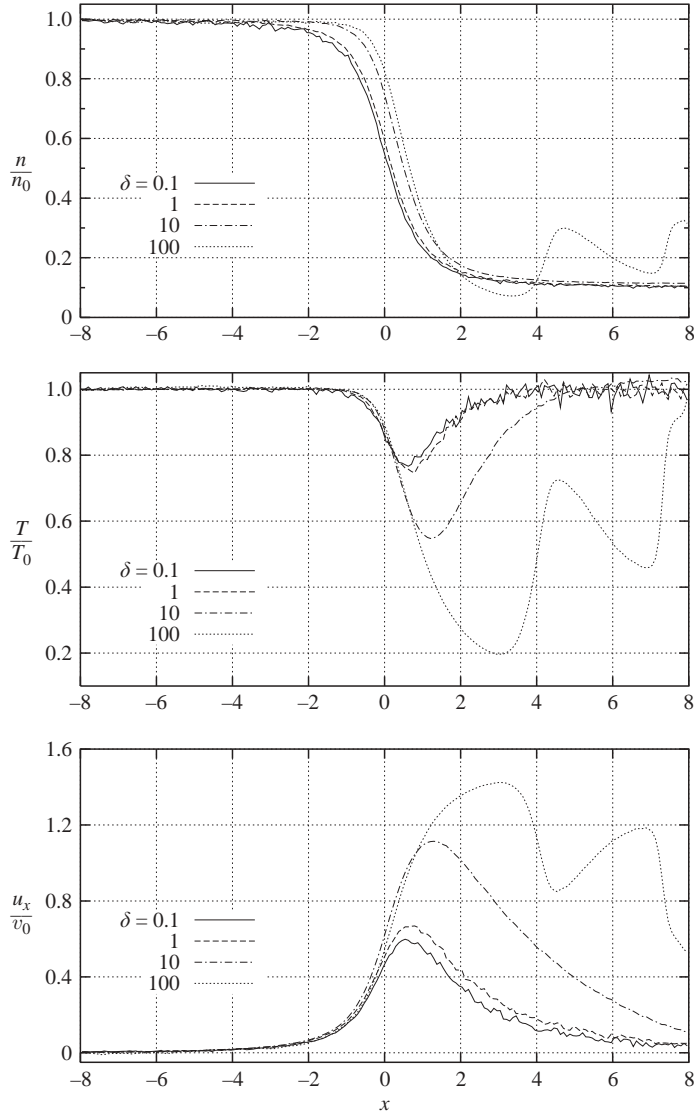


FIGURE 9. Distributions of density, temperature and bulk velocity along the orifice axis at $P_1/P_0 = 0.1$.

decays monotonically to zero. At $\delta = 100$ the velocity reaches its maximum values in the points where the temperature has its minimum values.

Qualitatively, the behaviours of the density, temperature and velocity for the pressure ratio $P_1/P_0 = 0.5$ are similar to those for $P_1/P_0 = 0.1$ at $\delta = 0.1, 1$ and 10 with the difference that the density varies from n_0 to $0.5n_0$ and the variations of the temperature and velocity are smaller. In the hydrodynamic regime ($\delta = 100$) the spatial derivatives of all quantities have a sharp variation i.e. $\partial/\partial x$, at $x/a = 1$. A calculation showed that at this point the local Mach number reaches its maximum value, which is very close to unity.

For the small pressure drop, i.e. $P_1/P_0 = 0.9$, just quantitative differences of the axial distributions from those for $P_1/P_0 = 0.5$ are observed. The density varies from

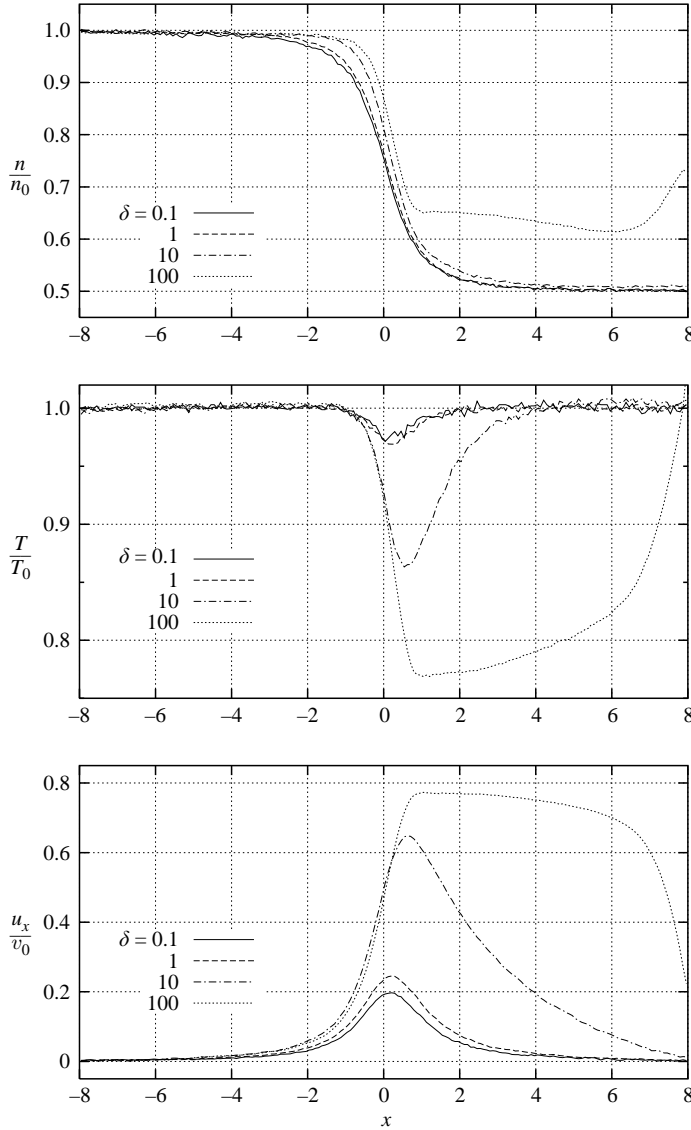


FIGURE 10. Distributions of density, temperature and bulk velocity along the orifice axis at $P_1/P_0=0.5$.

n_0 to $0.9n_0$, the temperature variation is about 3% at $\delta = 100$ and about 1% at $\delta = 10$. For $\delta = 0.1$ and 1 the temperature variation is of the order of the statistical scattering. The bulk velocity is significantly smaller than the local sound velocity.

Since in the hydrodynamic regime ($\delta = 100$) at the pressure ratios $P_1/P_0 = 0.1, 0.5$ and 0.9 the macroscopic quantities do not decay smoothly to their equilibrium values additional calculations were carried out with a larger computational domain, i.e. the length of the downflow container was increased up to $L_1 = 16$, see figure 1. A comparison of these results with those obtained for $L_1 = 8$ is shown in figures 12, 13 and 14 for $P_1/P_0 = 0.1, 0.5$ and 0.9 respectively, where the solid lines represents the result for $L_1 = 16$ and the circles correspond to those for $L_1 = 8$. It can be seen that the results obtained for $L_1 = 8$ are affected by the boundary just in the small

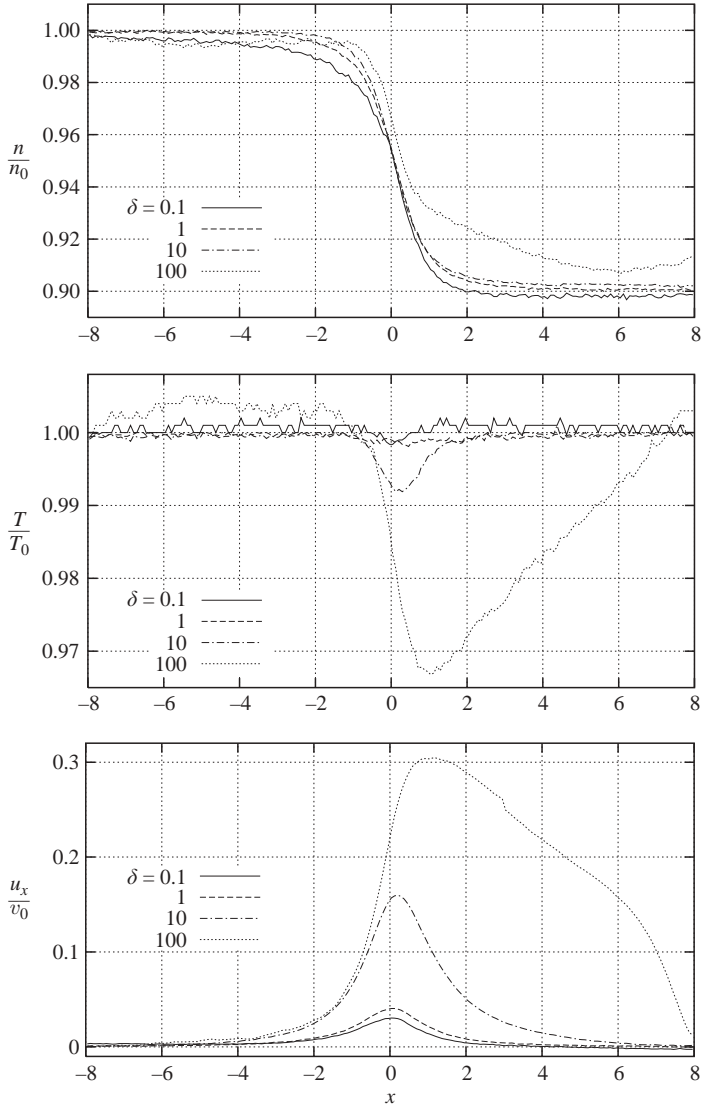


FIGURE 11. Distributions of density, temperature and bulk velocity along the orifice axis at $P_1/P_0 = 0.9$.

region $7 \leq x/a \leq 8$ for $P_1/P_0 = 0.1$ and in the region $6 \leq x/a \leq 8$ for $P_1/P_0 = 0.5$ and $P_1/P_0 = 0.9$, where the flow stagnation occurs. Moreover, figure 12 shows that the density, temperature and bulk velocity have several points of maximum and minimum before the decay to the equilibrium values.

8. Concluding remarks

The mass flow rate through a thin orifice for four values of the pressure ratio and for the whole range of gas rarefaction was calculated by the direct simulation Monte Carlo method. The values of the pressure ratio embrace the case of outflow into vacuum, i.e. choked flow, and the case of a small pressure drop, i.e. non-choked flow.

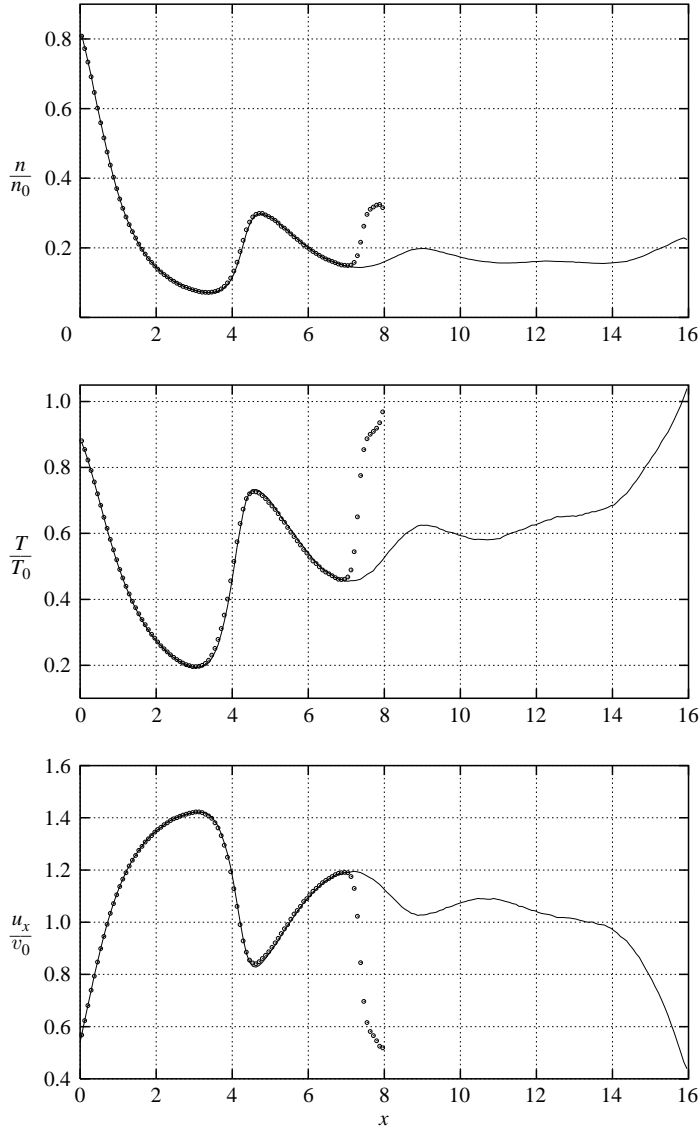
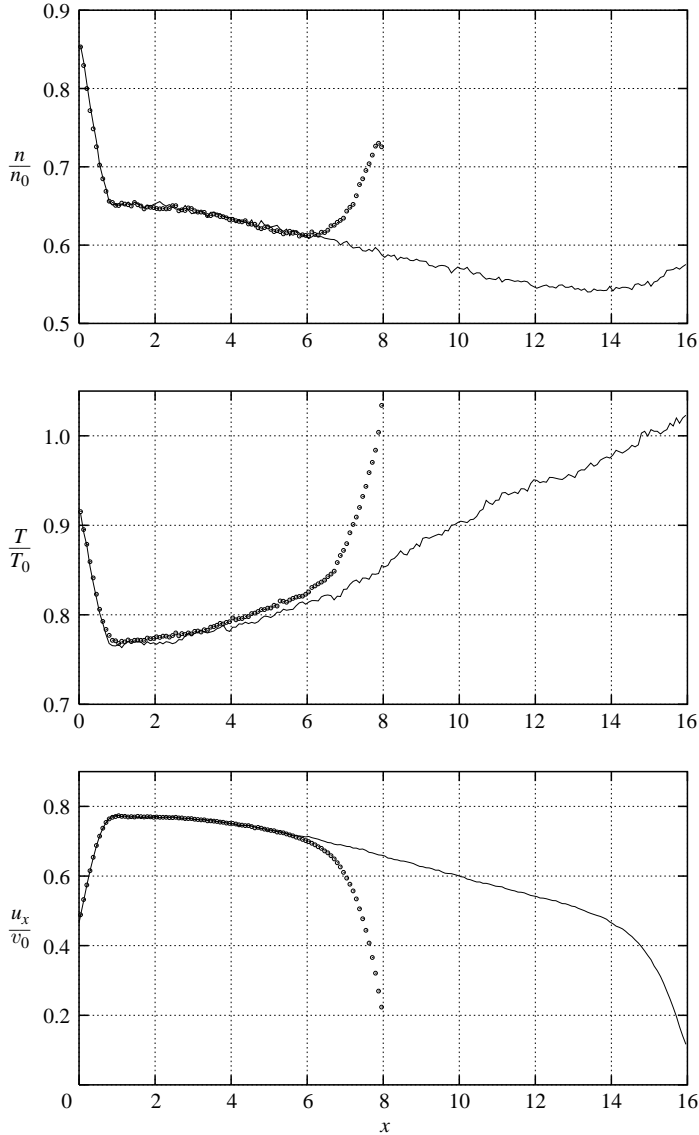


FIGURE 12. Distributions of density, temperature and bulk velocity along the orifice axis at $P_1/P_0 = 0.1$ and $\delta = 100$: \circ , $L_1 = 8$; —, $L_1 = 16$.

It was shown that at any pressure ratio the flow rate tends to a constant value in the hydrodynamic regime, which is established at rarefaction parameter δ equal to 50. The most significant variation of the flow rate occurs in the range of the rarefaction parameter from 0.5 to 50.

Good agreement was observed between the present numerical results and experimental data available in the open literature. It should be noted, however, that there is a lack of reliable experimental data on orifice flow for wide ranges of the gas rarefaction and intermediate values of the pressure ratio.

To reach a reasonable numerical accuracy related to the statistical scattering, the number of samples must drastically increase on decreasing the pressure drop, i.e. when the pressure ratio P_1/P_0 approaches unity. In the range $0.9 \leq P_1/P_0 \leq 1$ the


 FIGURE 13. As figure 12 but at $P_1/P_0 = 0.5$.

computer time increases so significantly that the DSMC method becomes inefficient and the problem must be solved on the basis of numerical calculation of the kinetic equation.

Near the hydrodynamic regime vortices appear in the downflow container if the pressure ratio differs from zero. In the hydrodynamic regime the gas flow begins to form a strong jet just beyond the orifice. Along this jet the variation of the macroscopic qualities is not monotonic at $P_1/P_0 = 0.1$.

In the future, the numerical code used to calculate the present results will be generalized to simulate the gas flow through short tubes. This will allow us to evaluate the influence of the partition thickness on the flow rate over the whole range of gas rarefaction.

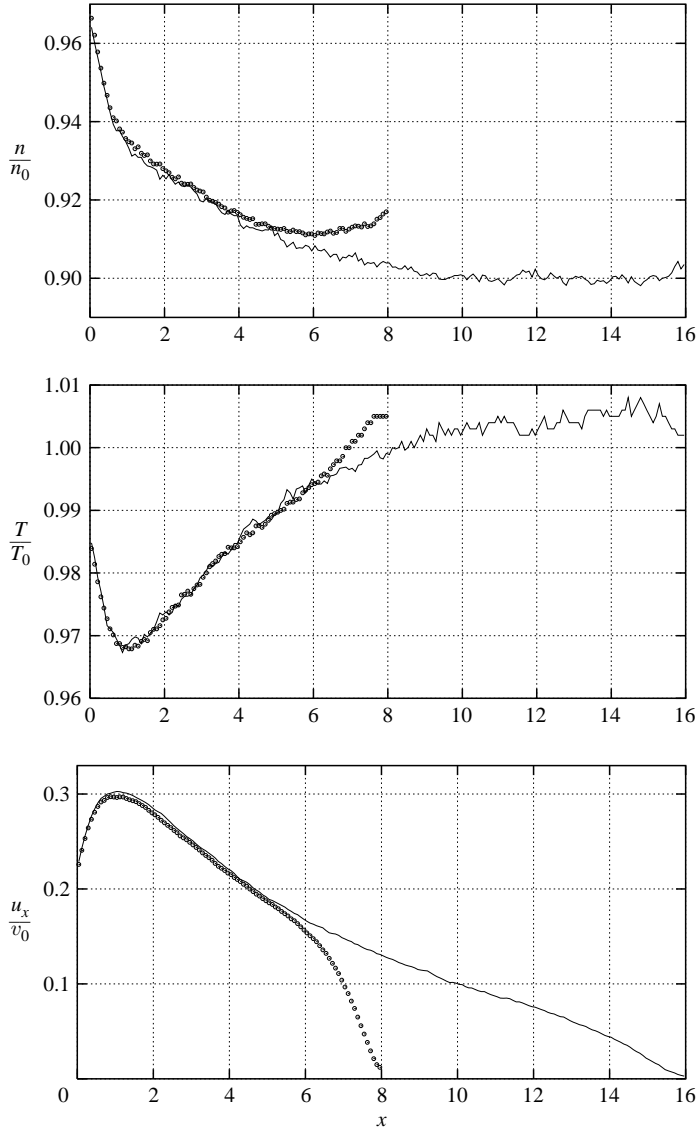


FIGURE 14. As figure 12 but at $P_1/P_0=0.9$.

The research of the author is supported by the Conselho Nacional de Desenvolvimento Científico e Tecnológico (CNPq, Brazil). The author thanks Professor W. Jitschin for providing his experimental results in tables.

REFERENCES

- AKTAS, O., ALURU, N. R. & RAVAIOLI, U. 2001 Application of a parallel DSMC technique to predict flow characteristics in microfluidic filters. *J. Microelectromech. Systems* **10**, 538–549.
- ALDER, G. M. 1979 The numerical solution of choked and supersonic ideal gas flow through orifices and convergent conical nozzles. *J. Mech. Engng Sci.* **21**, 197–203.
- BARASHKIN, S. T., PORODNOV, B. T. & CHEMAGIN, M. F. 1977a Experimental investigation of flows and direction diagrams for outflow of gas into vacuum through capillaries of various lengths. *Zh. Prikl. Mekh. Tekh. Fiz.* **4**, 74–80 (in Russian).

- BARASHKIN, S. T., PORODNOV, B. T. & SUETIN, P. E. 1977*b* Outflow of gas into vacuum through an orifice. *Zh. Tekh. Fiz.* **47**, 199–202 (in Russian).
- BERMAN, A. S. 1965 Free molecule transmission probabilities. *J. Appl. Phys.* **36**, 3356.
- BIRD, G. A. 1994 *Molecular Gas Dynamics and the Direct Simulation of Gas Flows*. Oxford University Press.
- BORISOV, S. F., NEUDACHIN, I. G., PORODNOV, B. T. & SUETIN, P. E. 1973 Flow of rarefied gases through an orifice for small pressure drop. *Zh. Tekh. Fiz.* **43**, 1735–1739 (in Russian).
- CERCIGNANI, C. 1988 *The Boltzmann Equation and its Application*. Springer.
- CERCIGNANI, C. & LAMPIS, M. 1971 Kinetic model for gas-surface interaction. *Transport Theory Statist. Phys.* **1**, 101–114.
- CERCIGNANI, C. & SHARIPOV, F. 1992 Gaseous mixture slit flow at intermediate Knudsen numbers. *Phys. Fluids A* **4**, 1283–1289.
- DANILATOS, G. D. 2001 Direct simulation Monte Carlo study of orifice flow. In *Rarefied Gas Dynamics* (ed. B. T. J. & M. A. Gallis), pp. 924–932. AIP.
- DANILATOS, G. D., PHILLIPS, M. R. & NAILON, J. V. 2001 Electron beam current loss at the high-vacuum-high-pressure boundary in the environmental scanning electron microscope. *Microscopy Microanal.* **7**, 397–406.
- DUSHMAN, S. 1962 *Scientific Foundation of Vacuum Technique*, 2nd edn. John Wiley & Sons.
- FUJIMOTO, T. & USAMI, M. 1984 Rarefied gas flow through a circular orifice and short tubes. *Trans. ASME: J. Fluids Engng* **106**, 367–373.
- HASEGAWA, M. & SONE, Y. 1991 Rarefied gas flow through a slit. *Phys. Fluids A* **3**, 466–477.
- HASIMOTO, H. 1958 On the flow of a viscous fluid past a thin screen at small Reynolds numbers. *J. Phys. Soc. Japan* **13**, 633–639.
- JAMISON, A. J., KETSDEVER, A. D. & MUNTZ, E. P. 2002 Gas dynamic calibration of a nano-Newton thrust stand. *Rev. Sci. Instrum.* **73**, 3629–3637.
- JITSCHIN, W., RONZHEIMER, M. & KHODABAKHSHI, S. 1999 Gas flow measurement by means of orifices and venturi tubes. *Vacuum* **53**, 181–185.
- JITSCHIN, W., WEBER, U. & HARTMANN, H. K. 1995 Convenient primary gas flow meter. *Vacuum* **46**, 821–824.
- LIEPMANN, H. W. 1961 Gas kinetics and gas dynamics of orifice flow. *J. Fluid Mech.* **10**, 65–79.
- LINDEN, H. R. & OTHMER, D. F. 1949 Air flow through small orifices in the viscous region. *Trans. ASME* **71**, 765–772.
- MATÉ, B., GRAUR, I. A., ELIZAROVA, T., CHIROKOV, I., TEJEDA, G., FERNANDEZ, J. M. & MONTERO, S. 2001 Experimental and numerical investigation of an axisymmetric supersonic jet. *J. Fluid Mech* **426**, 177–197.
- MATÉ, B., TEJEDA, G. & MONTERO, S. 1998 Raman spectroscopy of supersonic jets of CO₂: Density, condensation, and translational, rotational and vibrational temperatures. *J. Chem. Phys.* **108**, 2676–2685.
- NARASIMHA, R. 1961 Orifice flow of high Knudsen numbers. *J. Fluid Mech.* **10**, 371–384.
- PEKERIS, C. L. & ALTERMAN, Z. 1957 Solution of the Boltzmann-Hilbert integral equation. II. The coefficients of viscosity and heat conduction. *Proc. Natl Acad. Sci.* **43**, 998–1007.
- PERRY, J. A. J. 1949 Critical flow through sharp-edged orifices. *Trans. ASME* **71**, 757–764.
- PORODNOV, B. T., SUETIN, P. E., BORISOV, S. F. & AKINSHIN, V. D. 1974 Experimental investigation of rarefied gas flow in different channels. *J. Fluid Mech.* **64**, 417–437.
- RAMOS, A., MATÉ, B., TEJEDA, G., FERNÁNDEZ, J. M. & MONTERO, S. 2000 Raman spectroscopy of hypersonic shock waves. *Phys. Rev. E* **62**, 4940–4945.
- ROSCOE, R. 1949 The flow of viscous fluid round plane obstacles. *Phil. Mag.* **40**, 338–351.
- ROTENBERG, A. & WEITZNER, H. 1969 Nearly free flow through an orifice. *Phys. Fluids* **12**, 1573–1581.
- ROTH, A. 1976 *Vacuum Technology*. North-Holland.
- SAZHIN, O. V., BORISOV, S. F. & SHARIPOV, F. 2001 Accommodation coefficient of tangential momentum on atomically clean and contaminated surfaces. *J. Vac. Sci. Technol. A* **19**, 2499–2503, erratum: **20**, 957 (2002).
- SHAKHOV, E. M. 1974 Solution of axisymmetrical problems of the rarefied gas theory by the method of finite differences. *Zh. Vychislitel'noy Matem. Matem. Fiz.* **14**, 970–981 (in Russian).
- SHARIPOV, F. 1996 Rarefied gas flow through a slit: Influence of the gas-surface interaction. *Phys. Fluids* **8**, 262–268.

- SHARIPOV, F. 1997 Non-isothermal rarefied gas flow through a slit. *Phys. Fluids* **9**, 1804–1810.
- SHARIPOV, F. 2001 Rarefied gas flow through a thin orifice. In *Rarefied Gas Dynamics* (ed. T. J. Bartel & M. A. Gallis), pp. 494–501. AIP.
- SHARIPOV, F. 2002a Application of the Cercignani-Lampis scattering kernel to calculations of rarefied gas flows. I. Plane flow between two parallel plates. *Eur. J. Mech. B/ Fluids* **21**, 113–123.
- SHARIPOV, F. 2002b Rarefied gas flow into vacuum through a thin orifice. Influence of the boundary conditions. *AIAA J.* **40**, 2006–2008.
- SHARIPOV, F. 2003a Application of the Cercignani-Lampis scattering kernel to calculations of rarefied gas flows. II. Slip and jump coefficients. *Eur. J. Mech. B/ Fluids* **22**, 133–143.
- SHARIPOV, F. 2003b Application of the Cercignani-Lampis scattering kernel to calculations of rarefied gas flows. III. Poiseuille flow and thermal creep through a long tube. *Eur. J. Mech. B/ Fluids* **22**, 145–154.
- SHARIPOV, F. & SELEZNEV, V. 1998 Data on internal rarefied gas flows. *J. Phys. Chem. Ref. Data* **27** (3), 657–706.
- SREEKANTH, A. K. 1965 Transition flow through short circular tubes. *Phys. Fluids* **8**, 1951–1956.
- SZWEMIN, P., SZYMAŃSKI, K. & JOUSTEN, K. 1999 Monte Carlo study of a new PTB primary standard for very low pressure. *Metrologia* **36**, 562–564.
- WILLIS, D. R. 1965 Mass flow through a circular orifice and a two-dimensional slit at high Knudsen numbers. *J. Fluid Mech.* **21**, 21–31.